Sub-Rayleigh-diffraction-bound quantum imaging

Vittorio Giovannetti,[1] Seth Lloyd,[2] Lorenzo Maccone,[3] and Jeffrey H. Shapiro[2]

[1]*NEST-CNR-INFM and Scuola Normale Superiore, Piazza dei Cavalieri 7, I-56126, Pisa, Italy*
[2]*MIT, Research Laboratory of Electronics, 77 Massachusetts Avenue, Cambridge, Massachusetts 02139, USA*
[3]*QUIT, Dipartimento di Fisica "A. Volta," Universitá Pavia, via Bassi 6, I-27100 Pavia, Italy*
and Institute for Scientific Interchange, I-10133 Torino, Italy

The spatial resolution of an imaging apparatus is limited by the Rayleigh diffraction bound, a consequence of the imager's finite spatial extent. We show some N-photon strategies that permit resolution of details that are smaller than this bound, attaining either a $1/\sqrt{N}$ enhancement (standard quantum limit) or a $1/N$ enhancement (Heisenberg-like scaling) over standard techniques. In the incoherent imaging regime, the methods presented are loss resistant, since classical light sources suffice. Our results may be of importance in many applications: microscopy, telescopy, lithography, metrology, etc.

PACS number(s): 42.50.Dv, 03.67.−a, 42.30.Va

Quantum effects have been used successfully to provide resolution enhancement in imaging procedures. Among the many proposals that have been made [1], arguably the most famous is the quantum lithography procedure [2]. These methods take advantage of the fact that the effective wavelength of a multiphoton light state is shorter than its electromagnetic field wavelength: the light generation, propagation, and detection can be performed at optical wavelengths, where it is simple to manipulate, whereas the quantum correlations in the employed states allow one to perform imaging at the shorter multiphoton wavelength. Such proposals are then based on entangled or squeezed light sources, as entanglement or squeezing are necessary for efficient quantum enhancements [3]. If, however, efficiency considerations are dropped, it is also possible to employ classical-state light sources and post-selection at the detection stage to filter desirable quantum states from the classical light [4]. In fact, in many practical situations efficiency considerations do not play any role, as the quantum enhancement is typically of the order of the square root of the number of entangled systems [3], whereas in practical situations the complexity of generating the required quantum states has a much worse scaling. Many post-selection imaging procedures employing only classical light sources have been proposed and analyzed [5–17], and cover a wide range of interesting situations. Analogous methods have been employed successfully also in fields not directly related to imaging [18].

Here we show how one can achieve a resolution enhancement beyond what the apparatus' structural limits impose for conventional imaging, i.e., the Rayleigh diffraction bound x_R. In particular we show that employing appropriate light sources together with N-photon coincidence photodetection yields a resolution $\sim x_R/\sqrt{N}$. A resolution $\sim x_R/N$ can also be obtained by introducing, at the lens, a device that is opaque when it is illuminated by fewer than N photons. The first type of enhancement—a $1/\sqrt{N}$ standard quantum limit (SQL) for imaging—is an N-photon quantum process, but it is roughly equivalent to the classical procedure of averaging the arrival positions of N photons that originate from the same point on the object. The second type of

enhancement—a $1/N$ Heisenberg-like scaling for imaging—is a quantum phenomenon that derives from treating the N photons as a single field of N-times higher frequency. In the incoherent imaging regime, both methods can tolerate arbitrary amounts of loss at the expense of reduced efficiency but without sacrificing resolution. To compare the performance of our technique with conventional imaging methods, an explicit setup that uses visible light will be analyzed in detail, and shows that the decrease in efficiency is manageable for $N \lesssim 5$. It is worth stressing that, via proper scaling of the system parameters, our analysis can be applied to a broader context (not necessarily involving optical frequencies).

We start by reviewing some basics of conventional imaging. Then we discuss the SQL coherent and incoherent sub-Rayleigh imaging procedures. We conclude with a procedure achieving the $1/N$ Heisenberg scaling.

Rayleigh bound. Consider monochromatic imaging using a circular-pupil thin lens of radius R and focal length f that is placed at a distance D_o from an object of surface area $\mathcal{A}$, and at a distance D_i from the image plane, where $1/D_0 + 1/D_i = 1/f$. In conventional imaging, the object is illuminated by an appropriate (spatially coherent or incoherent) source and the image plane distribution of the light intensity, corresponding to the probability of detecting a photon at each image-plane point $\vec{r}_i$, is recorded. For photodetectors whose spatial-resolution area $\mathcal{S}$ and temporal-resolution time Δt are sufficiently small, the preceding probability is $P_1(\vec{r}_i) \simeq (\eta \mathcal{S} c \Delta t) \langle E_i^{(-)}(\vec{r}_i, t) E_i^{(+)}(\vec{r}_i, t) \rangle$, where angular brackets denote ensemble average over the illumination's state, η is the detector quantum efficiency, and $E^{(+)} = [E^{(-)}]^\dagger$ is the positive-frequency component of the electric field. This field component obeys $E_i^{(+)}(\vec{r}_i, t) = \int d^3 \vec{k} \, \mathcal{E}_i^{(+)}(\vec{r}_i; \vec{k}) e^{-ikt/c} a(\vec{k})$, where $a(\vec{k})$ is the field annihilation operator for the optical mode with wave vector $\vec{k}$ and $\mathcal{E}_i^{(+)}$ is the solution to the associated Helmholtz equation at the image plane. The latter can be written in terms of the corresponding object-plane field $\mathcal{E}_o^{(+)}(\vec{r}_o, \vec{k}) = e^{i\vec{k}_t \cdot \vec{r}_o}$, where $\vec{k}_t$ is the transverse component of $\vec{k}$, using classical imaging equations. For monochromatic light in the paraxial regime $k_t \ll k$, it follows that [19,20]
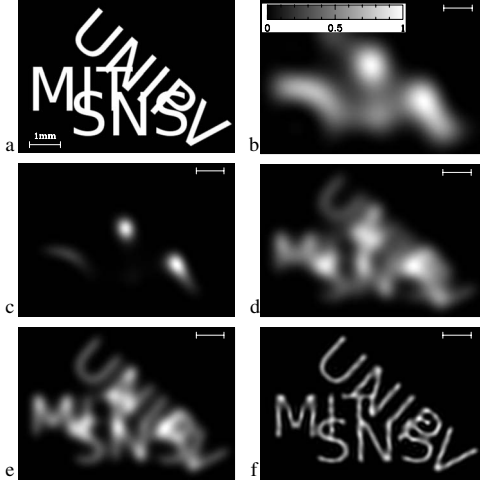
FIG. 1. Coherent imaging. (a) Object to be imaged. (b) Conventional coherent image (3) computed for $D_o/R=200$ (e.g., corresponding to $D_o=10$ cm and $R=0.5$ mm), $k=8.57\times10^5$ m^{-1} (red light), and $m=1$ (note that, modulo a rescaling, the same images would be found for any value of m). Owing to diffraction, no object details below the Rayleigh bound $x_R=0.89$ mm (segment in the top right corner of the pictures) are discernible in the image. (c) N-fold coincidence detection ($N=5$) through Eq. (6): resolution is not enhanced over the previous image despite the Nth-order compression of the point-spread function. (d) SQL reconstruction with illumination by the superposition of Fock states from Eq. (7) with $N=3$ and $\Delta k_t/k=0.1$. Sub-Rayleigh resolution is present. (e) The same as (d) for $N=5$; more resolution enhancement occurs. (f) Heisenberg-like coherent reconstruction from Eq. (11) with $N=5$; still further enhancement is evident. All plots are normalized so that the minimal and maximal intensities are 0 and 1, respectively.

$$\mathcal{E}_i^{(+)}(\vec{r}_i;\vec{k}) = \int \frac{d^2\vec{r}_o}{\mathcal{A}} A(\vec{r}_o)h(\vec{r}_i,\vec{r}_o)E_o^{(+)}(\vec{r}_o;\vec{k}), \qquad (1)$$

where $\vec{r}_i$ and $\vec{r}_o$ are two-dimensional vectors in the image and object planes, $A(\vec{r}_o)$ is the object aperture function [22], and $h(\vec{r}_i,\vec{r}_o)$ is the point-spread function of the imaging apparatus given by [12,19,20]

$$h(\vec{r}_i,\vec{r}_o) = \frac{R^2k^2\mathcal{A}}{4\pi D_o D_i}e^{i\vartheta}\text{somb}(Rk|\vec{r}_o+\vec{r}_i/m|/D_o), \qquad (2)$$

$\text{somb}(x)\equiv 2J_1(x)/x$ being the Airy function and $m=D_i/D_o$ the image magnification factor. The phase ϑ in Eq. (2) plays no role in the protocol, and can be neglected or compensated using standard imaging techniques [19].

Coherent imaging prevails when collimated coherent-state illumination is employed, i.e. [see Figs. 1(a) and 1(b)],

$$P_1^{(c)}(\vec{r}_i) = \eta Sc\Delta t I_o \left| \int \frac{d^2\vec{r}_o}{\mathcal{A}} A(\vec{r}_o)h(\vec{r}_i,\vec{r}_o) \right|^2, \qquad (3)$$

with $I_o\equiv\langle E_o^{(-)}E_o^{(+)}\rangle$ being the field intensity on the object plane. Incoherent imaging occurs when the object is illuminated by independent (monochromatic) beams propagating from all directions [see Figs. 2(a) and 2(b)] whence
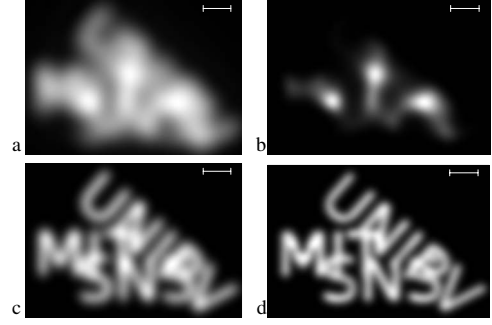

FIG. 2. Incoherent imaging of the object shown in Fig. 1(a) with the same parameters. (a), (b) Conventional incoherent images from Eq. (6) with $N=1$ and 5, respectively. The images are featureless blurs, because the Rayleigh bound x_R (segment in top right corner) is too large to resolve the details. (c), (d) Reconstruction via Eq. (10) using the mixture σ of coherent states for $N=3$ and 5, respectively. The price one has to pay for the increase in resolution of (c) and (d) is a reduction in intensity of the images by a factor 10^3 and 10^5, respectively (for the parameters given in the text).

$$P_1^{(\text{inc})}(\vec{r}_i) = \frac{\eta Sc\Delta t}{2\pi k^2\mathcal{A}}I_o \int \frac{d^2\vec{r}_o}{\mathcal{A}}|A(\vec{r}_o)h(\vec{r}_i,\vec{r}_o)|^2. \qquad (4)$$

When the lens radius R is sufficiently large, Eqs. (4) and (3) produce inverted, magnified, perfect images of the object, because $R^2\text{somb}(R|\vec{x}|)\to 4\pi\delta^{(2)}(\vec{x})$ for $R\to\infty$ [19]. For small R, the convolution integrals in Eqs. (4) and (3) produce blurred images. The amount of blurring can be gauged through the Rayleigh bound: for a point source at $\vec{r}_o$ in the object plane, the resulting image-plane intensity is proportional to $\text{somb}^2(Rk|\vec{r}_o+\vec{r}_i/m|/D_o)$, which comprises a pattern of circular fringes in $\vec{r}_i$ that are centered on $-m\vec{r}_o$. The radius of the first fringe, $x_R\simeq 0.61\times 2\pi mD_o/(kR)$, about $-m\vec{r}_o$ encloses $\sim 84\%$ of the light falling on the image plane [20]. Intuitively, the image of an extended object is then a weighted superposition of radius-x_R circles off centered about each $-m\vec{r}_o$. This is the Rayleigh bound; using conventional imaging techniques, one cannot resolve details smaller than x_R.

SQL. The main idea of SQL sub-Rayleigh imaging is to use an appropriate light source and to replace intensity measurement with spatially resolving N-fold coincidence detection strategies. The probability of detecting N photons at position $\vec{r}_i$ on the image plane is [21]

$$P_N(\vec{r}_i) \simeq \frac{(\eta Sc\Delta t)^N}{N!}\langle[E_i^{(-)}(\vec{r}_i,t)]^N[E_i^{(+)}(\vec{r}_i,t)]^N\rangle, \qquad (5)$$

which can be accomplished by means of doppleron absorbers [23], photon-number resolving detectors, or N-fold coincidence counting (which exploits the full photon statistics: the N value needs not be predetermined). Note that multiphoton detection alone does not guarantee sub-Rayleigh performance. In fact, for the coherent imaging of Eq. (3), N-photon detection gives

$$P_N(\vec{r}_i) = [P_1^{(c)}(\vec{r}_i)]^N/N!. \qquad (6)$$

The N in the exponent gives an N-fold compression of the fringes in the point-spread function. It amounts to taking the Nth power of the light intensity, which is formally equivalent to a classical post-processing of the signal of Eq. (3). As shown in Fig. 1(c) no resolution enhancement is obtained using only N-photon detection: an appropriate light source is also needed.

A first example of such an input source is a superposition of N-photon Fock states, focused in a small area $s \equiv (\pi\Delta k_t^2)^{-1} \ll \mathcal{A}$ centered at positions $\vec{r}_o$ on the object

$$|\psi\rangle \equiv \frac{1}{\sqrt{\mathcal{M}}} \int d^2\vec{r}_o |N\rangle_{\vec{r}_o}, \quad |N\rangle_{\vec{r}_o} \equiv \frac{1}{\sqrt{N!}}[b^\dagger(\vec{r}_o)]^N|0\rangle, \quad (7)$$

where $b(\vec{r}_o)$ is the annihilator of the associated localized spatial mode [24] and $\mathcal{M} \simeq \frac{4\mathcal{A}}{\Delta k_t^2}$ is the normalization. Inserting this state into Eq. (5), we find

$$P_N(\vec{r}_i) \simeq \frac{\Delta k_t^2 \mathcal{A}}{4\pi} \xi^N \left| \int \frac{d^2\vec{r}_o}{\mathcal{A}} Q^N(\vec{r}_i, \vec{r}_o) \right|^2,$$

$$Q(\vec{r}_i, \vec{r}_o) \equiv \int \frac{d^2\vec{r}}{\mathcal{A}} A(\vec{r}) h(\vec{r}_i, \vec{r}) F_{\Delta k_t}(|\vec{r}_o - \vec{r}|), \qquad (8)$$

where $F_{\Delta k_t}(x) \equiv \pi\Delta k_t^2 \mathcal{A} \, \mathrm{somb}(\Delta k_t x)$, and $\xi \equiv \eta \frac{\Delta\omega\Delta t}{\pi\Delta k_t^2 \mathcal{A}} \frac{\mathcal{S}}{\mathcal{A}}$ is a dimensionless quantity that is typically very small because of the monochromatic ($\Delta\omega\Delta t \ll 1$) and focusing assumptions ($\pi\Delta k_t^2 \mathcal{A} \gg 1$). Equation (8) can be simplified by assuming $D_o/R \gg k/\Delta k_t$, which implies that each number state in the superposition is focused to a spot much smaller than the object-plane Rayleigh limit of the lens. In this case, h can be extracted from the integral yielding $Q(\vec{r}_i, \vec{r}_o) \simeq h(\vec{r}_i, \vec{r}_o)\tilde{A}(\vec{r}_o)$ with $\tilde{A}(\vec{r}_o) \equiv \int \frac{d^2\vec{r}_o}{\mathcal{A}} A(\vec{r}) F_{\Delta k_t}(|\vec{r}_o - \vec{r}|)$. Now Eq. (8) becomes

$$P_N^{(c)}(\vec{r}_i) \simeq \frac{\Delta k_t^2 \mathcal{A}}{4\pi} \xi^N \left| \int \frac{d^2\vec{r}_o}{\mathcal{A}}[\tilde{A}(\vec{r}_o) h(\vec{r}_i, \vec{r}_o)]^N \right|^2, \qquad (9)$$

which, contrary to Eq. (6), cannot be obtained through classical post-processing of P_1. It generalizes coherent imaging (3) to N-photon detection. The point-spread function that governs spatial resolution is now h^N—which is narrower than h—so that when $A(\vec{r}_o) \simeq \tilde{A}(\vec{r}_o)$ there is an enhancement in resolution, see Figs. 1(d) and 1(e).

An analogous generalization for incoherent imaging is obtained by replacing the state Eq. (7) with an incoherent mixture of focused Fock states, i.e., $\rho = \int \frac{d^2\vec{r}_o}{\mathcal{A}} |N\rangle_{\vec{r}_o}\langle N|$. In this case, Eq. (9) becomes

$$P_N^{(\mathrm{inc})}(\vec{r}_i) \simeq \xi^N \int \frac{d^2\vec{r}_o}{\mathcal{A}} |\tilde{A}(\vec{r}_o)|^{2N} |h(\vec{r}_i, \vec{r}_o)|^{2N}, \qquad (10)$$

which generalizes Eq. (4) to N-photon detection. The attainable resolution is shown in Figs. 2(c) and 2(d).

The Fock states employed in Eqs. (7) and (10) are highly sensitive to loss and are quite difficult to create. Nevertheless, N-fold incoherent imaging can be realized with loss-resistant and easy to create light sources, which are prefer-

able in most situations. One can use an incoherent mixture of coherent states that randomly illuminate all points on the object: $\sigma = \int \frac{d^2\vec{r}_o}{\mathcal{A}} |\alpha\rangle_{\vec{r}_o}\langle\alpha|$, where $|\alpha\rangle_{\vec{r}_o} \equiv \exp[\alpha b^\dagger(\vec{r}_o) - \alpha^* b(\vec{r}_o)]|0\rangle$. Equation (10) still applies with an extra multiplicative factor of $|\alpha|^{2N}/(N!)$. The state σ can be easily prepared by shining a highly focused laser beam on the object, one point at the time. This state is robust to loss, as the loss parameter η just takes $|\alpha\rangle$ into $|\sqrt{\eta}\alpha\rangle$. An arbitrary amount of loss can be tolerated—without sacrificing resolution—simply by increasing $|\alpha|$. In the same way, we can overcome the reduction in efficiency (exponential in N) associated with the low intensities of the signals that come from the factor ξ^N. To show that this procedure is practical, we calculate the reduction in image intensity for realistic values of the parameters $\eta = 10^{-3}$, $\Delta\omega\Delta t \sim 10^{-1}$, $\mathcal{S} = \mathcal{A} \times 10^{-6}$ (and the values given in the figure captions for the remaining ones). Then, the ratio between the maximum intensities of our method and the classical procedure can be straightforwardly evaluated from the coefficients in front of the function h of Eq. (2) and in front of the probability (10). It follows that for a pulsed laser with an easily attainable $|\alpha|^2 \sim 5 \times 10^{11}$, the light intensity reaching the image plane is $\sim 10^5$ times lower for $N = 5$ than a classical procedure with the same illumination: the resolution increase of Fig. 2(d) comes at the cost of a 10^5 reduction in the absolute intensity. Nonetheless, a good quality image can easily be obtained: the $\sim 10^7$ N-photon events necessary for imaging can be obtained in $\sim 10^5$ laser pulses, i.e., typically in a small fraction of a second.

The amount of resolution gain from the procedures detailed above can be roughly estimated by gauging by narrowing of the point-spread function h that results from taking its Nth power. For instance, one can evaluate the radius $x_R(N)$ that contains 84% of the area under somb^{2N}. Numerical analysis shows that $x_R(N)/x_R \sim 1/\sqrt{N}$, which suggests an SQL [3] for imaging. This should be taken only as a rough estimate, as $x_R(N)$ is also the radial dimension of a pointlike object imaged using the post-processing strategy of Eq. (6). For more extended objects, the resolution enhancement depends also on Δk_t. The $1/\sqrt{N}$ scaling exposes the classical nature of this enhancement: the same effect can be attained by averaging the arrival positions of N photons at the image plane. This is surely advantageous over N-photon detection in many situations, but it is impractical for lithography or film photography, and it cannot reproduce the coherent imaging case of Eq. (9). Moreover, from general principles [1,3] one would expect that also a $1/N$ Heisenberg-like scaling is achievable, i.e., a resolution $\sim x_R/N$, not achievable with classical strategies.

Heisenberg-like scaling. The $1/N$ scaling can be obtained by treating the N photons as a single entity of N-times higher frequency. This situation can be simulated, at least in principle, by inserting immediately in front of the lens a screen divided into small sections each of area s_F such that, if less than N photons reach one section, they are absorbed, otherwise they are coherently transmitted. Such a screen does not currently exist but, in principle, one could be built, e.g., by using doppleron materials [23]. Then, if the object is illuminated by the focused coherent states described above, only N

photons that originate at $\vec{r}_o$, successfully transit the screen within one of its area-s_F segments, and get detected at $\vec{r}_i$ can contribute to the image at that point. Again loss just reduces the efficiency, but not the resolution. In this case, the operators $[E_i^{(+)}(\vec{r}_i,t)]^N$ of the N-photon absorption probability (9) (or N-fold coincidence detection) are approximately given by [25]

$$[E_i^{(+)}(\vec{r}_i,t)]^N \simeq \gamma \int \frac{d^2\vec{r}_o}{\mathcal{A}} h_N(\vec{r}_i,\vec{r}_o)[\tilde{A}(\vec{r}_o)b(\vec{r}_o)]^N. \quad (11)$$

Here h_N is obtained from Eq. (2) by replacing k with Nk, i.e., h_N is the point-spread function for photons having N-times higher frequency than the illumination; and γ accounts for the spatial resolution of the doppleron screen, i.e., it is of

order $(\frac{s_F}{\pi R^2})^N$. Equation (11) describes the absorption of N frequency-ω photons that originated near $\vec{r}_o$ and then propagated through the imaging apparatus as if they were a single frequency-$N\omega$ photon. It gives rise to coherent and incoherent images that are formally equivalent to those of Eqs. (3) and (4) for a light beam of wave number Nk, thus realizing the Heisenberg-like scaling of an N-fold resolution improvement over the Rayleigh bound, albeit with an even worse efficiency than the N-photon detection methods given above—see Fig. 1(f).

[1] E.g., see M. I. Kolobov, Rev. Mod. Phys. **71**, 1539 (1999).

[2] A. N. Boto, P. Kok, D. S. Abrams, S. L. Braunstein, C. P. Williams, and J. P. Dowling, Phys. Rev. Lett. **85**, 2733 (2000).

[3] V. Giovannetti, S. Lloyd, and L. Maccone, Science **306**, 1330 (2004); Phys. Rev. Lett. **96**, 010401 (2006); S. L. Braunstein, Nature (London) **440**, 617 (2006).

[4] K. L. Pregnell and D. T. Pegg, J. Mod. Opt. **51**, 1613 (2004).

[5] H. P. Yuen and J. H. Shapiro, IEEE Trans. Inf. Theory **24**, 657 (1978).

[6] P. R. Hemmer, A. Muthukrishnan, M. O. Scully, and M. S. Zubairy, Phys. Rev. Lett. **96**, 163603 (2006); A. Muthukrishnan, M. O. Scully, and M. S. Zubairy, J. Opt. B: Quantum Semiclassical Opt. **6**, S575 (2004).

[7] D. Korobkin, and E. Yablonovitch, Opt. Eng. **41**, 1729 (2002).

[8] C. Thiel *et al.*, e-print arXiv:quant-ph/070.1024.

[9] S. J. Bentley and R. W. Boyd, Opt. Express **12**, 5735 (2004).

[10] M. Zhang *et al.*, e-print arXiv:quant-ph/0612060.

[11] K. Wang and D.-Z. Cao, Phys. Rev. A **70**, 041801(R) (2004).

[12] Y. Shih, IEEE J. Sel. Top. Quantum Electron. **13**, 1016 (2007).

[13] E. Yablonovitch and R. B. Vrijen, Opt. Eng. **38**, 334 (1999).

[14] A. Pe'er *et al.*, Opt. Express **12**, 6600 (2004).

[15] B. I. Erkmen and J. H. Shapiro, Phys. Rev. A **77**, 043809 (2008).

[16] *Quantum Imaging*, edited by M. I. Kolobov (Springer, New York, 2006).

[17] L. A. Lugiato, A. Gatti and E. Brambilla, J. Opt. B: Quantum Semiclassical Opt. **4**, S176 (2002).

[18] F. S. Cataliotti, R. Scheunemann, T. W. Hansch, and M. Weitz, Phys. Rev. Lett. **87**, 113601 (2001); C. Skornia, J. von Zanthier, G. S. Agarwal, E. Werner, and H. Walther, Phys. Rev.

A **64**, 063801 (2001); M. W. Mitchell, J. S. Lundeen, and A. M. Steinberg, Nature (London) **429**, 161 (2004); K. J. Resch, K. L. Pregnell, R. Prevedel, A. Gilchrist, G. J. Pryde, J. L. OBrien, and A. G. White, Phys. Rev. Lett. **98**, 223601 (2007).

[19] J. W. Goodman, *Introduction to Fourier Optics* (McGraw-Hill, New York, 1988).

[20] M. Born and E. Wolf, *Principles of Optics* (Cambridge Univ. Press, Cambridge, 1999).

[21] L. Mandel and E. Wolf, *Optical Coherence and Quantum Optics* (Cambridge Univ. Press, Cambridge, 1995).

[22] The function A measures the attenuation of the light due to the object. We assume A to be independent of $\vec{k}$; the generalization to a $\vec{k}$-dependent A is straightforward.

[23] J. J. Tollett, J. Chen, J. G. Story, N. W. M. Ritchie, C. C. Bradley, and R. G. Hulet, Phys. Rev. Lett. **65**, 559 (1990); N. P. Bigelow and M. G. Prentiss, *ibid.* **65**, 555 (1990).

[24] It is given by $b(\vec{r}_o) \equiv \int \frac{d\omega}{\sqrt{\Delta\omega}} \int \frac{d^2\vec{k}_t}{\sqrt{\pi\Delta k_t^2}} e^{i\vec{k}_t\cdot\vec{r}_o} a(\vec{k})$, where the frequency integration is performed over a small bandwidth $\Delta\omega$ around the mean frequency $\omega = kc$ and the wave-vector integration is performed over $|\vec{k}_t| \leq \Delta k_t$. The exact expression for $\mathcal{M}$ is $\int d^2\vec{r}_o \int d^2\vec{r}_o' F_{\Delta k_t^2}^N(|\vec{r}_o - \vec{r}_o'|)/\mathcal{A}^N$, which, for highly localized modes $\pi\Delta k_t^2 \mathcal{A} \gg 1$, gives $\mathcal{M} \simeq 4A/\Delta k_t^2$.

[25] Use the screen-to-lens transfer function to write $[E_i^{(+)}(\vec{r}_i,t)]^N$ as a convolution of the products $E_l^{(+)}(\vec{r}_l^{(1)},t) \cdots E_l^{(+)}(\vec{r}_l^{(N)},t)$, $E_l^{(+)}(\vec{r}_l,t)$ being the electric field on the screen. The screen removes all contributions but those for which the $\vec{r}_l^{(j)}$ fall in the same area-s_F region. Equation (11) follows by writing the resulting operator as a convolution of $E_o^{(+)}(\vec{r}_o^{(1)},t) \cdots E_o^{(+)}(\vec{r}_o^{(N)},t)$ through the object-to-lens transfer function, and noting that for focused sources it is approximated by $[b(\vec{r}_o^{(1)})]^N$.